Research article

Single-cell mapping of peripheral blood mononuclear cells reveals key transcriptomic changes favoring coronary artery lesion in IVIG-resistant Kawasaki disease

Yuanzheng Zheng [a,1], Yan Zhou [b,1], Di Zhu [c,1], Xing Fu [d,1], Cao Xie [e], Shuna Sun [a], Guoyou Qin [f], Mei Feng [c], Chenglong Liu [c], Qingtong Zhou [c,g], Fang Liu [a], Chen Chu [a], Feng Wang [a], Dehua Yang [b,g], Ming-Wei Wang [c,g,h,**], Yonghao Gui [a,*]

[a] Children's Hospital of Fudan University, National Children's Medical Center, Shanghai, 201102, China
[b] The National Center for Drug Screening, Shanghai Institute of Materia Medica, Chinese Academy of Sciences, Shanghai, 201203, China
[c] Department of Pharmacology, School of Basic Medical Sciences, Fudan University, Shanghai, 200032, China
[d] Accuramed Technology (Shanghai) Ltd., Shanghai, 200233, China
[e] School of Pharmacy, Fudan University, Shanghai, 201203, China
[f] School of Public Health, Fudan University, Shanghai, 200032, China
[g] Research Center for Deepsea Bioresources, Sanya, Hainan, 572025, China
[h] Department of Chemistry, School of Science, The University of Tokyo, Tokyo, 113-0033, Japan

ARTICLE INFO

ABSTRACT

Background: Intravenous immunoglobulin (IVIG)-resistant Kawasaki disease (KD) poses a considerable challenge to patients and their families due to its severe complications. Previous researches have highlighted the critical role of immune disorders in its pathogenesis. However, fragmented studies based on isolated cases hinder a comprehensive understanding of this deadly illness. This study aimed to explore the overall landscape of peripheral blood mononuclear cells (PBMCs) in IVIG-resistant KD patients using single-cell RNA sequencing (scRNA-seq).
Methods: The scRNA-seq was used to characterize the transcriptomic profiles of IVIG-resistant KD patients, IVIG-responsive KD patients, and healthy controls. Data quality control (QC) and subsequent analysis were conducted using various R packages. These included DoubletFinder and Harmony for QC, Seurat and SingleR for identifying and annotating major cell types, ggpubr for calculating and visualizing the percentages of each cell type, Seurat for characterizing differentially expressed genes (DEGs) between groups, pheatmap for visualizing the DEGs, clusterProfiler for performing Gene Ontology (GO) enrichment analysis of DEGs, scRepertoire for TCR and BCR data analysis, Monocle for assessing cell differentiation trajectories, and CellChat for intercellular interaction evaluation.
Results: High-quality single-cell transcriptome data from 12 participants were analyzed, including five with IVIG-resistant KD, four with IVIG-responsive KD, and three healthy controls. We identified 10 major cell types and observed that the differentiation of CD8$^+$ effector T cells was impeded in IVIG-resistant KD patients with coronary artery lesion (CAL) according to cell differentiation trajectory analysis. Subsequent cell communication analysis demonstrated that

---

* Corresponding author.
** Corresponding author. Department of Pharmacology, School of Basic Medical Sciences, Fudan University, Shanghai, 200032, China.
E-mail addresses: mwwang@simm.ac.cn (M.-W. Wang), yhgui@fudan.edu.cn (Y. Gui).
[1] These authors contributed equally.

myeloid cluster with high expression of *LCN2*, *S100P*, and *LTF* played a key role, potentially signaling through MIF-CD74/CXCR4 and MIF-CD74/CD44 ligand-receptor pairs.

Conclusion: Complex immunopathological changes occur during the development of CAL in IVIG-resistant KD. Stunted differentiation of CD8$^+$ effector T cells is noted in KD-CAL. Interactions between myeloid cells and T cells activates multiple inflammatory signaling pathways, with ligand-receptor pairs, including MIF-CD74/CXCR4 and MIF-CD74/CD44, potentially playing crucial roles.

1. Introduction

Kawasaki disease (KD) is an acute vasculitis with an unknown cause that primarily affects children under five years old [1]. It is prevalent in over 60 countries and regions, with the highest incidence in east Asia, rising annually [2]. For instance, in Japan, the incidence rose from 243.1 per 100,000 children <4 years in 2011 to 359 in 2018 [3,4], and in South Korea from 254.5 per 100,000 children <5 years in 2008 to 334.7 in 2017 [5]. Coronary artery lesion (CAL) is the most common complication of KD, making KD a major cause of children acquired heart disease [6]. Patients with coronary artery involvement face a high risk of cardiovascular events such as coronary artery thrombosis, stenosis, and even myocardial infarction during follow-up [7,8]. Although intravenous immunoglobulin (IVIG) has significantly reduced coronary artery aneurysm (CAA) incidence, approximately 10 %–20 % of KD patients do not respond to IVIG and are consequently at a higher risk of CAA [9].

IVIG resistance is defined as the continuation or return of fever at least 36 h following the completion of IVIG infusion [2,10]. Despite years of research, many problems remain unsolved, necessitating further investigation into the immunological basis of IVIG-resistance [11]. CAA are the most common sequela of KD, with a particularly worrisome prognosis for giant CAA (GCAA) [12]. Markers of endothelial injury may persist long after the initial onset, and severe complications such as thrombosis and myocardial infarction may develop secondary to CAA [13]. A previous study showed that 25 years after the onset of KD, 16 % of patients with GCAA experienced myocardial infarction, 59 % underwent interventional or surgical treatment of coronary arteries, and at 30 years after the onset, the survival rate was only 88 % [14]. Evidence suggests ongoing vascular inflammation and long-term endothelial cell dysfunction in CAA years after KD onset, and that a history of KD in childhood is likely related to coronary atherosclerosis in adulthood [8,15].

Transcript abundance and gene expression studies will enhance the understanding of the mechanisms underlying IVIG-resistant KD and CAA-complicated KD. The advancement of single-cell RNA sequencing (scRNA-seq) technology has significantly improved our ability to analyze the transcriptional profiles of various cell types [16]. In the present study, scRNA-seq was utilized to examine peripheral blood mononuclear cells (PBMCs) from KD patients and healthy controls. Differences in cellular and molecular characteristics between IVIG-resistant and IVIG-responsive KD, as well as between CAA-complicated and non-CAA KD, were analyzed using network analysis. The findings offer holistic insights into the nature of IVIG-resistant and CAA-associated KD.

2. Methods

2.1. Study participants

Patients with KD and healthy controls were enrolled between September 15 and December 31, 2021. A total of 12 participants from the Children's Hospital of Fudan University were involved in this study, including five patients with IVIG-resistant KD, four with IVIG-responsive KD, and three healthy controls. This study was reviewed and approved by the institutional Ethics Committee of the Children's Hospital of Fudan University, with the IRB protocol number: 2021-369. Written informed consent was obtained from the legal guardians of all participants. All KD patients were diagnosed according to the criteria established by the American Heart Association (AHA) and Japan Circulation Society (JCS) [2,7]. All patients received standard treatment with a single dose of 2 g/kg/day IVIG in combination with acetylsalicylic acid (ASA), as recommended by the AHA guidelines. IVIG-resistant KD was characterized by recurrent or persistent fever at least 36 h after the completion of the initial IVIG infusion, in line with the AHA guidelines [2]. All blood specimens from patients for scRNA-seq were collected within 36–72 h after initial IVIG therapy. Healthy controls were age-matched and had no history of autoimmune disease or recent infection.

2.2. Single-cell preparation and sequencing

2.2.1. PBMC isolation and single-cell preparation

All peripheral blood samples were drawn into EDTA anti-coagulant tubes and swiftly transported on ice to the laboratory within 30 min to preserve cell viability. PBMCs were separated by performing density-gradient sedimentation using Ficoll-Paque (GE Healthcare, USA). The cells at the intermediate interface were extracted, and the resulting pellet was washed twice with PBS. To remove red blood cells, the cell pellet was treated with a red blood cell lysis buffer (Sigma-Aldrich, USA) for 5 min at room temperature, followed by centrifugation at $250 \times g$ and 4 °C for 5 min. The purified cells were then resuspended in 200–500 μL PBS containing 0.4 % BSA (Sigma-Aldrich) and passed through a 40 μm cell strainer. Cell concentration and viability were assessed using a LUNA automated cell counter (Logos Biosystems, Korea) and the cell suspension was diluted with PBS containing 0.04 % BSA to achieve a concentration 700-1200

cells/μL.

2.2.2. 10 × Genomics library preparation and sequencing

Single cells were loaded and barcoded using a 10x Chromium Controller (10x Genomics, USA), with an aim of at 5000 cells per sample for each chip position. Following this, library construction for scRNA-seq was performed using the Chromium Single Cell 5′ Library and Gel Bead kit (V2) from 10x Genomics, following the manufacturer's protocols. The Chromium Single Cell V(D)J Amplification kit, along with the Human TCR and BCR Amplification kits, were used to generate scBCR-seq and scTCR-seq libraries. The 5′ gene expression and TCR/BCR libraries were then sequenced on a NovaSeq 6000 system (Illumina, USA) until adequate saturation was achieved.

2.2.3. scRNA-seq data processing

The scRNA-seq reads in FASTQ format were aligned to the human reference genome (GRCh38) using the 10x Genomics Cell Ranger Pipeline (version 5.0.1) with default settings to produce gene-barcode matrices. Each element of the gene-barcode matrix represents the number of unique molecular identifiers (UMIs) associated with the gene and barcode. Filtered gene expression matrices containing only detected cell-associated barcodes were subsequently loaded into the Seurat (v4.0.4) R toolkit for further analysis and visualization.

2.2.4. Quality control, normalization and dimensional reduction

Potential doublets in each library were identified using the DoubletFinder (v2.0.3) R package, and removed. Cells with mitochondrial gene content exceeded 5 % were then discarded. Cells with a UMI proportion of hemoglobin subunit genes greater than 5 % were removed, to eliminate erythrocytes. Multiple gene-barcode matrices from all samples were merged using Seurat and processed using the Log Normalization method. The top 2000 variable genes were identified using the *FindVariableFeatures* function. The data corresponding to these genes were then normalized, scaled, and centered with the *ScaleData* function. Principal Component Analysis (PCA) was subsequently conducted on the processed data, analyzing 50 principal components. Based on the PCA dimensions, using the *RunHarmony* function from the Harmony (v0.1.0) R package, we integrated multiple samples and mitigate batch effects. The top 20 dimensions generated by harmony were subsequently used for clustering and tSNE analysis by *FindNeighbors* and *RunTSNE* functions, respectively.

2.3. Clustering and cell type annotation

To identify gene expression markers for each cluster, the *FindClusters* function was used with a resolution of 0.8. Subsequently, the *FindAllMarkers* function, utilizing the Wilcoxon Rank-Sum test, was applied to detect these markers. The major cell types in the clusters were determined according to these known canonical marker gene expressions. Clusters assigned to the same cell type were merged. SingleR (v1.6.1) was employed with the Blueprint Encode Data reference dataset for automatic cell type annotation. B cell subtypes were annotated based on the SingleR results.

2.4. Cell type composition analysis

To determine significant differences in cell-type compositions across the groups, the percentages of each cell type per sample were calculated and visualized with boxplots using the R package ggpubr (v0.4.0). The Wilcoxon Rank-Sum test was employed to compare two independent groups, with statistical significance set at $P < 0.05$.

2.5. Differentially expressed gene and Gene Ontology (GO) analysis

The *FindMarkers* function in Seurat was used to identify differentially expressed genes (DEGs) between groups by utilizing the Wilcoxon Rank-Sum test. The average level of DEGs was calculated by *AverageExpression* function and visualized as a heatmap using the pheatmap (v 1.0.12) R package. The ClusterProfiler (v4.0.0) R package was utilized for GO enrichment analysis of the identified DEGs.

2.6. TCR and BCR analysis

The 10x Genomics Cell Ranger Pipeline (version 5.0.1) was employed to process single-cell V(D)J data with reference to vdj_GRCh38_alts_ensembl-5.0.0. Filtered contig annotation CSV files produced using the Cell Ranger Pipeline were loaded and combined using the *combine*TCR and *combine*BCR functions in the scRepertoire (v1.4.0) R package for TCR and BCR data, respectively. These functions integrated TCR and BCR contig annotations down to individual cell barcodes, identifying clonotypes using the CDR3 amino acid sequences. Cells with the same CDR3 sequence were considered to exhibit the same phenotype. The clone size of a unique clonotype was determined by counting the number of barcoded cells. TCR and BCR cell barcodes were matched with scRNA-seq data and cell type annotations in the Seurat object using the *combine*Expression functions of scRepertoire.

The proportions of expanded TCR/BCR clones with sizes greater than one, as well as the frequencies of expanded T and B cells, were calculated and compared between different groups using the Wilcoxon Rank-Sum test, with a significance threshold set at $P < 0.05$.

The expanded TCR clones of CD4$^+$ and CD8$^+$ T cell subtypes were further categorized into four groups based on their clone size:

2–5, 5–10, 10–20 and ≥ 20. The proportions of TCR clones and T cells within each clone size ranges were calculated and compared between the different groups. A similar approach was applied to the BCR clones and B cell subtypes. Additionally, we quantified the number of TCR clones shared between the two different T cell subtypes and compared them among the different groups.

2.7. Pseudotime analysis and cell-cell communication analysis

Monocle (version 3.0) was employed to construct a single-cell pseudo-time differentiation trajectory, allowing for the examination of differentiation patterns across various cell clusters. ScRNA-seq data were subsequently analyzed to investigate the cellular communication networks, with the R package CellChat used to visualize the communication among various cell types.

2.8. Clinical laboratory data collection

Blood count parameters, including hemoglobin (Hb), percentage of neutrophils, platelet (PLT) count, and white blood cell (WBC) count, and blood biochemical data, including alanine aminotransferase (ALT), albumin, aspartate aminotransferase (AST), C-reactive protein (CRP) and serum sodium levels, were collected. See Supplementary Materials for further details.

2.9. Statistical analysis

Continuous variables are presented as means ± standard deviation. To compare two groups, the Wilcoxon Rank-Sum test was used, while one-way analysis of variance (ANOVA) was employed for comparisons across multiple groups. Statistical significance was defined as $P < 0.05$, $*P < 0.05$, $**P < 0.01$, and $***P < 0.001$. Statistical analyses were conducted by SPSS version 20.0 (IBM Corporation, USA), while data visualization was performed using Prism software (version 8.0; GraphPad Software, USA).

3. Results

3.1. Clinical characteristics of the participants

Twelve participants including five with IVIG-resistant KD, four with IVIG-responsive KD, and three healthy controls, were recruited. Among the five patients with IVIG-resistant KD, two were complicated by CAL and three were not. None of the four IVIG-responsive patients had CAL complications. A flow-chart illustrating the participant selection process is presented in Fig. S1. The mean age of the participants at enrollment was 26 months (range 3–59 months). Additional details are available in Tables S1–S3.

The CRP level in IVIG-resistant KD patients was elevated compared to healthy controls, while WBC and AST showed an increasing trend before the standard 2 g/kg IVIG treatment relative to levels observed in IVIG-responsive patients and healthy controls (Fig. 1A and S2A). However, a decreasing trend of sodium, Hb, and albumin were observed in IVIG-resistant patients prior to the standard 2 g/kg IVIG treatment (Fig. 1B). After IVIG treatment, the IVIG-resistant group exhibited higher levels of WBC, percentage of neutrophils, CRP, and ALT, but lower levels of Hb and albumin than the IVIG-responsive group and healthy controls (Fig. 1C and D, and S2B).

### 3.2. scRNA-seq profile of PBMCs in IVIG-resistant patients with CAL

After quality control, a total number of 60,332 PBMCs from KD patients with IVIG-response, KD patients with IVIG-resistance, and healthy controls were used in the downstream analysis (Fig. 2A). Cell clusters were well segregated and the top ten cell subsets were identified with distinct gene expression patterns (Fig. 2B). The expression levels of curated feature genes across the top ten subsets is shown in Fig. 2C, and the number of each cell subsets was illustrated in Fig. 2D, CD4$^+$ naïve T led the way with 19,002 cells, followed by naïve B with 10,621 cells, and then CD8$^+$ naïve T with 7508 cells. Cell proportions were analyzed in each sample (Fig. 2E and F), and a decreasing trend in the proportion of CD8$^+$ effector T cells was observed in patients with IVIG-resistance and CAL.

The cell proportion of representative cell populations between the groups was compared across IVIG-responsive patients, IVIG-resistant patients, and healthy controls (Fig. S3A), however, there was no statistical significance. In IVIG-resistant patients combined with CAL, there was a higher percentage of naïve B cells and CD4$^+$ naïve T cells, accompanied by a decreased percentage of CD8$^+$ effector T cells, monocytes, natural killer (NK) cells, neutrophils and plasma cells, compared with IVIG-responsive KD patients and IVIG-resistant patients without CAL. Moreover, patients in the IVIG-resistant CAL, IVIG-resistant without CAL, and IVIG-responsive groups had a reduced percentage of CD4$^+$ helper T cells compared with healthy controls (Fig. S3B). In summary, a decreasing trend of several cell populations, particularly CD8$^+$ effector T cells, was observed in patients with IVIG-resistance and CAL.

3.3. GO analysis in IVIG-resistant patients with CAL

To identify genes involved in the immune response during CAL formation, differential expression analysis was performed, and the number of DEGs between the different cell populations of CAL and non-CAL patients was analyzed. As shown in Fig. 3A, most of the DEGs were down-regulated. Monocytes showed the highest number of DEGs, followed by CD8$^+$ effector T cells and NK cells. The functions of these DEGs was examined using GO analysis.

Gene set enrichment analysis revealed that different cell subsets shared similar DEGs. Genes associated with T cell activation, leukocyte mediated immunity, and response to virus were enriched in monocytes, CD8$^+$ effector T cells, and NK cells (Fig. 3B, C, and
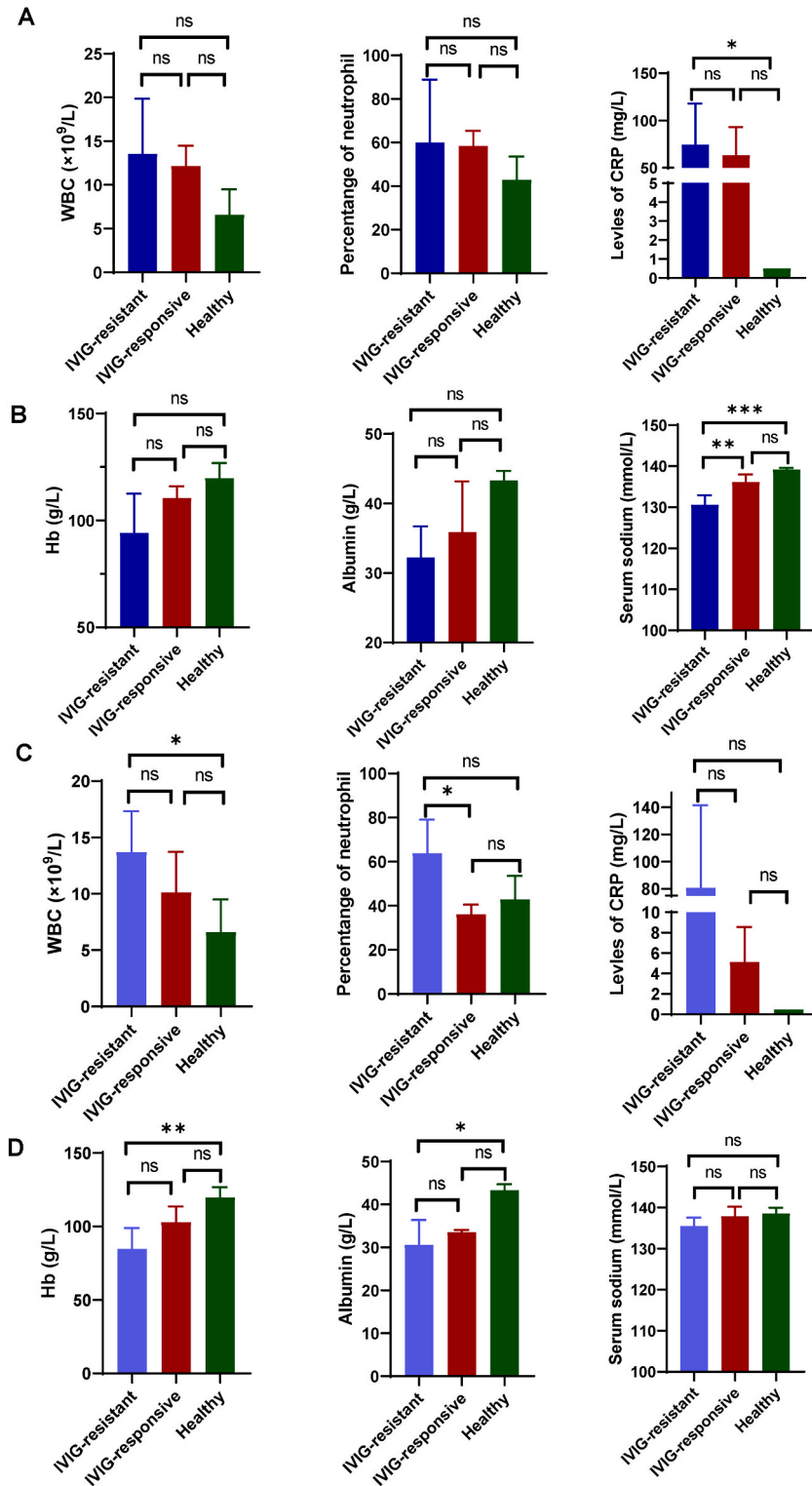
(caption on next page)

Fig. 1. Clinical characteristics of the participants
A. The number of white blood cell (WBC), the proportion of neutrophils, and serum levels of C-reaction protein (CRP) in peripheral blood of healthy controls and KD patients who are either IVIG-resistant or IVIG-responsive before the initial IVIG treatment. **B.** Hemoglobin (Hb), albumin, and serum sodium in peripheral blood of healthy controls and KD patients who are either IVIG-resistant or IVIG-responsive before initial IVIG treatment. **C.** WBC count, the proportion of neutrophils, and serum levels of CRP in peripheral blood of healthy controls and KD patients who are either IVIG-resistant or IVIG-responsive after initial IVIG treatment. **D.** Hb, albumin, and serum sodium in peripheral blood of healthy controls and KD patients who are either IVIG-resistant or IVIG-responsive after initial IVIG treatment.

3D). Meanwhile, genes related to regulation of cytokine-mediated signaling pathway were enriched in monocytes, CD8$^+$ effector T cells, as well as neutrophils (Fig. 3B, C, and 3E). Additionally, genes related to cytokine production, and regulation of response to biotic stimulus were enriched in monocytes, CD8$^+$ effector T cells, NK cells, and neutrophils (Fig. 3B, C, 3D, and 3E). These findings suggest that alterations in the expression of these pathway-related genes across various immune cells may significantly contribute to the occurrence and progression of CAL.

Since the expression of genes related to T cell activation was markedly down-regulated in several cell types, differentiation relationships among different T cell clusters were investigated, and single-cell pseudo-time differentiation trajectories were constructed. In the pseudo-time analysis, the differentiation trajectory of four distinct T cell clusters was defined, and stunted differentiation of CD8$^+$ effector T cells was identified in the CAL group (Fig. 3F). Overall, these results indicate that the gene expression related to T cell activation was significantly altered, and CD8$^+$ T cell differentiation was hindered in the CAL group.

3.4. Analysis of T/B cell with clonal TCR/BCR in patients with CAL

After IVIG treatment, there was an enrichment of CD8$^+$ effector cells carrying clonal TCRs in all four groups; however, no significant clonal expansion was observed among the other T cell types. A downward trend in clonal expansion of CD8$^+$ effector T cells and CD4$^+$ helper T cells was observed in the CAL group compared with other groups (Fig. 4A). In addition, clonal expansion of CD4$^+$ naïve and CD8$^+$ naïve T cells showed a downward trend in the non-CAL group (Fig. 4A). B cells with clonal BCR size greater than one were also analyzed, and expansion of both memory and naïve B cells was observed in the CAL group (Fig. 4C).

As shown in Fig. 4B–E, the percentages of expanded TCR and BCR clones were evaluated. Consistent with the expanded T cells, an upward trend of expanded TCR clones in CD8$^+$ effector T cells was observed in four groups, while there was no significant clonal expansion in other T cell subsets. The clonal expansion of TCR clones in CD8$^+$ effector and CD4$^+$ helper T cells showed a downward trend in CAL group. Different from B cell expansion, the percentage of expanded BCR clones in both memory B and naïve B cells decreased markedly in both the CAL and non-CAL groups. Collectively, these results further supported the retardation of CD8$^+$ T cell development and differentiation in the CAL group.

3.5. Crosstalk between CD8$^+$ T cells and myeloid cells in CAL patients

Given the observed inhibition of CD8$^+$ T cell development and the functional enrichment of DEGs in myeloid cells associated with T cell activation, we investigated the evolutionary relationship between CD8$^+$ T cells and myeloid cells. Re-cluster analysis of myeloid cells showed that cluster 3 was more prevalent in PBMCs from KD patients, whereas cluster 6 was predominant in healthy controls (Fig. 5A). The highly expressed genes for each myeloid cell cluster are shown in Fig. 5B. Evolutionary relationship analysis between myeloid and T cells demonstrated that cluster 3 evolved late in myeloid cells, and the differentiation of CD8$^+$ effector T cells was inhibited after cluster 3 evolution (Fig. 5C and D). Since clusters 3 and 6 differentiated into different states, branched expression analysis modeling (BEAM) was used to show the pseudo-temporal expression dynamics of specific representative genes. The top 100 fate-determining genes involved in pre-branch differentiation into two distinct cell fates are shown in Fig. 5E. Myeloid cluster 3, characterized by high expression of genes such as *LCN2*, *S100P*, and *LTF*, inhibited CD8$^+$ T cell differentiation (Fig. 5A, B, 5C, and 5D). The key genes that determined the fate of myeloid cluster 3 differentiation were genes related to interferon signaling pathway, including *IFIT2*, *IFIT3*, *IFITM1*, *ISG*, *IFITM2*, and *GBP5* (Fig. 5E). In summary, the interactions between myeloid cluster 3 cells and CD8$^+$ effector T cells may inhibit the differentiation of CD8$^+$ effector T cells.

To further explore the crosstalk between T cells and myeloid cells, we utilized CellChat, which revealed complex cell-cell interaction networks between these cell types (Fig. 6A and B and S5). We then explored the molecular mechanisms mediating cell-cell interactions in patients with CAL and calculated the attraction strength of the ligand-receptor pairs. Of the ligand-receptor pairs pertaining to myeloid and T cells, HLA-A-CD8A/CD8B, HLA-B-CD8A/CD8B, HLA-C-CD8A/CD8B, and HLA-E-CD8B were detected between myeloid and CD8$^+$ naïve T cells (Fig. 6C). Myeloid cells were found to preferentially express macrophage migration inhibitory factor (MIF), which binds to the CD74/CD44 complex, a signaling mediator implicated in autoimmune diseases, tumor growth, and metabolic diseases such as atherosclerosis [17–19]. Other ligand-receptor pairs involved in T cells and myeloid cells interactions included MIF-CD74/CXCR4 and RETN-CAP1. These results indicate that HLA and MIF may interact with certain integrins to promote CAL in IVIG-resistant patients.

3.6. Crosstalk between NKT cells and myeloid cells in CAL patients

The results revealed cell-cell interaction networks between natural killer T (NKT) and myeloid cells. The number of interaction factors varied among groups, but a higher number of interactions between NKT cells and myeloid cluster 8 was observed in patients
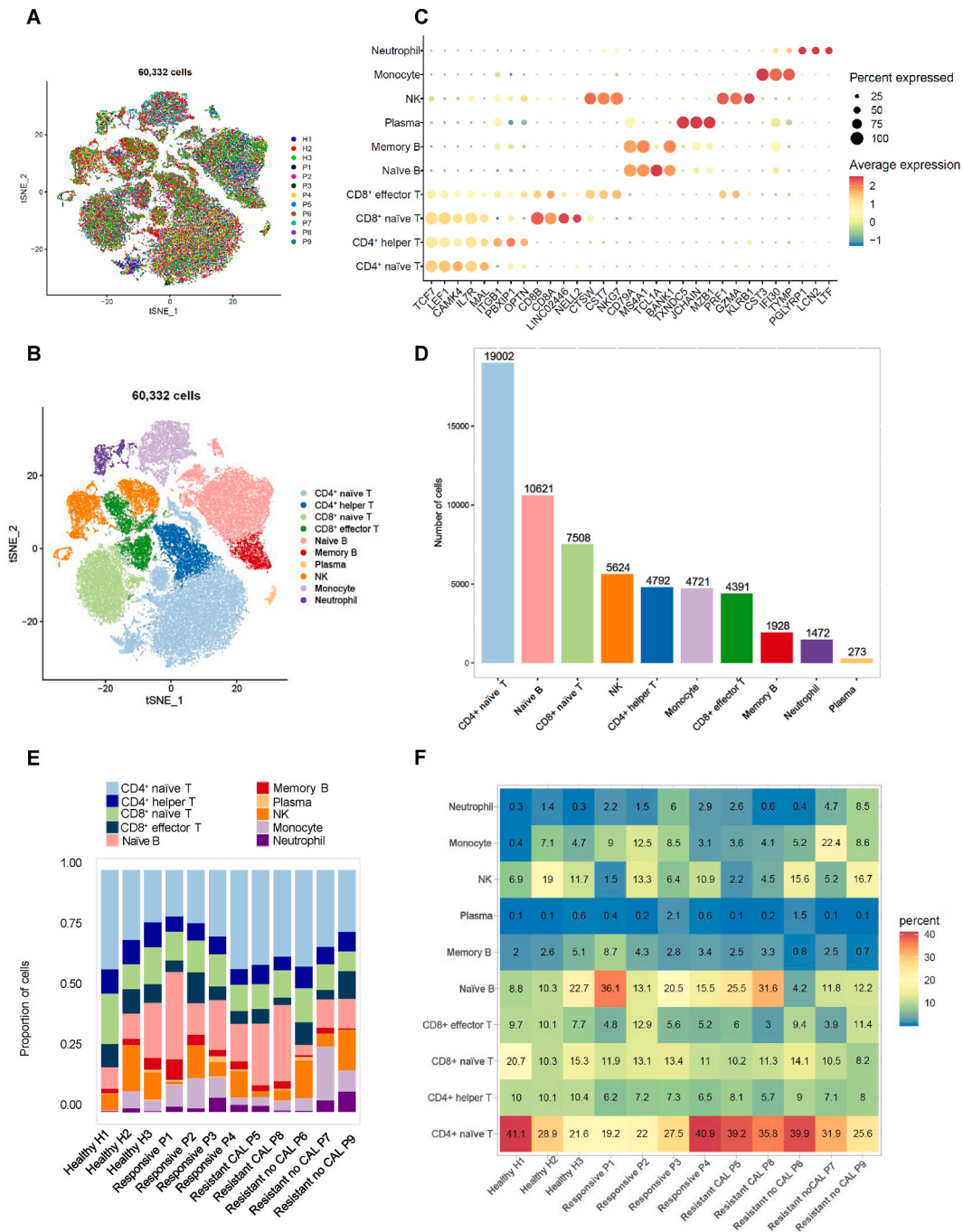
Fig. 2. Presentation of top ten cell types identified by scRNA-seq
A. Two-dimensional t-SNE visualization of expression profile clusters of PBMCs in healthy controls, IVIG-responsive, and IVIG-resistant patients. Each point represents an individual cell, color-coded by sample number. **B.** t-SNE visualization of expression profile clusters of PBMCs in healthy controls, IVIG-responsive, and IVIG-resistant patients. Each point represents an individual cell, color-coded by cell type. **C.** Cell type markers, along with dot plots displaying the expression of selected feature genes across 10 subsets. The size of each dot indicates the proportion of cells expressing a particular gene in the specified subset, while the color bar reflects the gene expression levels. **D.** Bar plot illustrating the number of the identified cell populations. **E.** Bar plot displaying the proportion of cell populations in each sample, colored according to cluster designation. **F.** Heat map showing the proportion of cell populations in each sample.
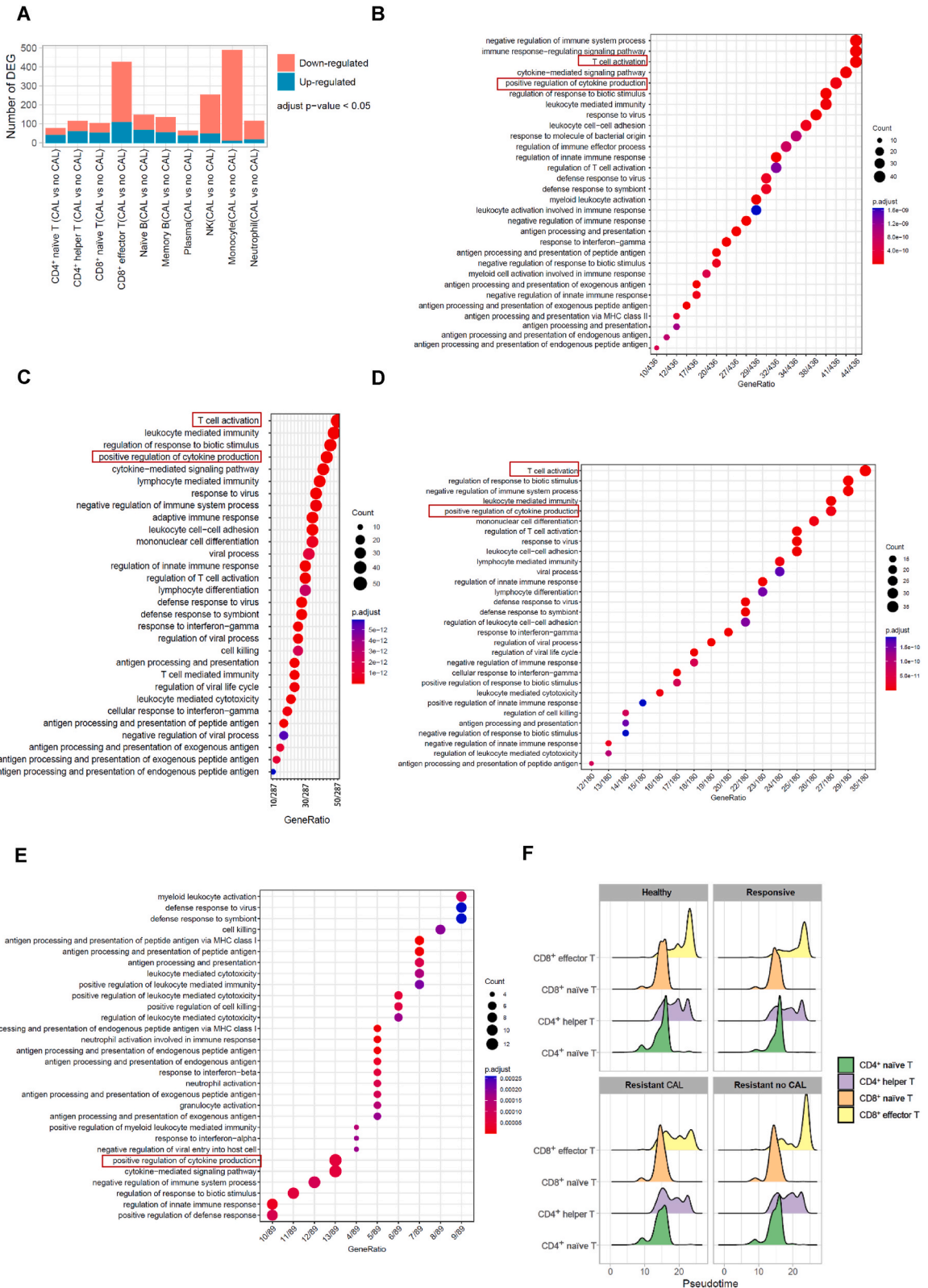
(caption on next page)

Fig. 3. Analysis of gene expression in IVIG-resistant patients with CAL

A. Number of DEGs in each cell population of IVIG-resistant CAL patients compared with IVIG-resistant non-CAL patients. **B-E.** GO analysis of down-regulated genes in monocytes (**B**), CD8^{+} effector T cells (**C**), NK cells (**D**) and neutrophils (**E**) from CAL patients compared to non-CAL patients. **F.** Pseudo-time analysis of T cell subsets in each group.

with CAL (Fig. 7A and B, and S6). In terms of the molecular mechanisms mediating NKT and myeloid cell interactions, two ligand-receptor pairs (MIF-CD74/CXCR4 and MIF-CD74/CD44) were involved (Fig. 7C), again suggesting that MIF may interact with certain integrins to promote the occurrence of CAL in IVIG-resistant patients.

4. Discussion

In this study, we demonstrated the PBMC atlas of patients with IVIG-resistant KD. The patients were further categorized into subgroups based on the presence or absence of CAL. Transcriptomic characteristics and interactions between different cell types were also investigated. In KD-CAL patients, genes associated with T-cell activation were down-regulated across several cell types, implying an inadequate T-cell immune response. Pseudo-time analysis suggested that myeloid cluster 3 cells, characterized by high expression of *LCN2*, *S100P*, and *LTF*, inhibited CD8^{+} T cells differentiation. The key genes determining the fate of myeloid cluster 3 differentiation were related to the interferon signaling pathway, including *IFIT2*, *IFIT3*, *IFITM1*, *ISG*, *IFITM2* and *GBP5*. This implies that the interferon signaling pathway was activated and could contribute to the development of CAL. The ligand-receptor pairs MIF-CD74/CD44and MIF-CD74/CXCR4 were repeatedly detected in immune cell communication among patients with CAL, suggesting their importance in CAL. Collectively, our results provide new perspectives for the clinical understanding of immunological changes in IVIG-resistant KD and suggest therapeutic targets for preventing CAL in these patients.

CD8^{+} T cells are known to play a protective role in various diseases, including infectious diseases such as COVID-19 [20,21], neurodegenerative disease [22], and cancer [23]. A previous study showed that a reduction in the percentage of CD8^{+} T cells, particularly effector memory CD8^{+} T cells, in patients with acute KD, with levels gradually rebounding after IVIG treatment [24]. Moreover, histopathological studies have revealed that valvulitis, a cardiovascular complication during the acute phase of KD, is characterized by the infiltration of cytotoxic T cells and macrophages in valve tissue [25]. However, information on the dynamic changes in T cells in KD-CAL patients is limited. In the present study, we observed impaired CD8^{+} T cell activation and maturation in CAL patients, suggesting CD8^{+} T cell dysfunction during the acute phase of KD. Multisystem inflammatory syndrome in children (MIS-C) shares similar clinical presentations and pathology with KD [26], and transcriptome-wide investigations have implicated that MIS-C patients show disruption in CD8^{+} T cell exhaustion, leading to severe and potentially fatal T cell immunopathology following viral infection; this finding has also been observed in an independent cohort of KD patients [27]. This highlights the similarities between the molecular etiologies of MIS-C and KD [27,28]. This is consistent with our findings, suggesting that CD8^{+} T cell dysfunction may lead to disease progression and play a key role in CAL formation. Furthermore, the ligand-receptor pairs MIF-CD74/CD44 and MIF-CD74/CXCR4 were detected in the crosstalk between CD8^{+} T cells and myeloid cells, suggesting that such an interaction may promote the occurrence of CAL in IVIG-resistant patients.

MIF is a pleiotropic cytokine implicated in various autoimmune diseases through its role in upstream immune regulation [17,29]. The cognate receptor of MIF is a two-component signaling complex consisting of the signal transducer CD44 and the ligand-binding protein CD74 [30,31]. After binding, the ligand-receptor MIF-CD77/CD44 can activate MAPK pathway and NF-κB pathways, respectively, regulating transcription of target genes to inhibit apoptosis, prolong cell survival and activate inflammation [31,32]. In our study, cell communication data from patients with KD-CAL showed that the MIF-CD77/CD44 and MIF-CD74/CXCR4 ligand-receptor pairs were present in interactions between myeloid cell and CD8^{+} T and NKT cells, suggesting a potential role of MIF in the development of CAL.

NKT cells are a unique subset of non-conventional T cells characterized by distinct TCRs and cell surface markers typically found on NK cells [33]. They are capable of recognizing both endogenous and exogenous glycolipid antigens displayed by the major histocompatibility complex class I-like molecule CD1d in association with β2-microglobulin [34]. NKT cells can be activated through several pathways including CD1d/TCR-dependent pathways. Upon activation, these cells rapidly produce various cytokines [35]; however, their roles in KD are largely unknown. Therefore, our findings provide clues for understanding the immune mechanisms underlying KD-CAL.

In summary, the present study presents a holistic immune atlas of IVIG-resistant KD, key transcriptomic characteristics, and interactions between different cell types related to CAL. This study provides preliminary information on the immunopathogenesis of IVIG-resistant KD complicated with CAL, which will advance the design and development of novel therapeutic strategies to combat this deadly disease.

5. Limitations

The small sample size, which may have contributed to the lack of statistical difference in cell subsets between the different groups, is one limitation of this study. Another limitation is that the study was conducted with human PBMCs, using only sc-RNA-seq to reach relevant conclusions, without verification experiments to support the results. Further studies could consider integrating sc-RNA-seq and bulk RNA-seq to identify key DEG sets, followed by experimental verification to strengthen the conclusion. The integration of genomic, transcriptomic, and proteomic studies will provide a more complete picture of the pathogenesis of IVIG-resistant KD.
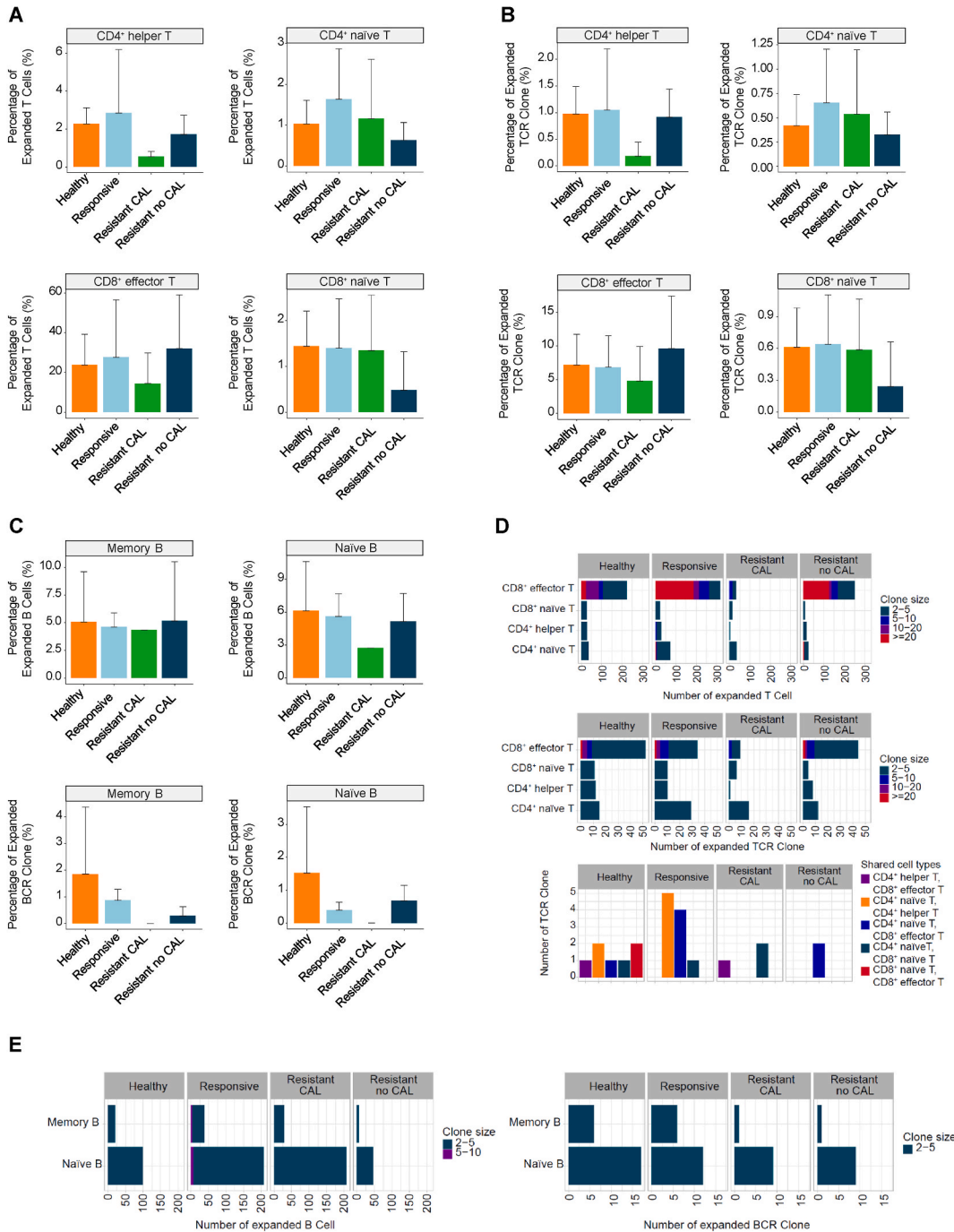
Fig. 4. Analysis of T/B cells with clonal TCR/BCR
A. The percentage of CD4$^+$ helper T cells, CD4$^+$ naïve T cells, CD8$^+$ effector T cells and CD8$^+$ naïve T cells exhibiting clonal expansion in healthy, IVIG-responsive, IVIG-resistant CAL, and IVIG-resistant non-CAL patients. **B.** The percentage of expanded TCR clones (clone size >1) in T cells across the four groups. **C.** The percentage of clonal expansion in naïve B and memory B cells between groups, as well as the percentage of expanded BCR clones (clone size >1) in B cells among groups. **D, E.** The number of expanded T cells, and TCR clones (**D**), and expanded B cells and BCR clones (**E**) in the four groups.

CRediT authorship contribution statement

Yuanzheng Zheng: Writing – original draft, Methodology, Formal analysis, Data curation. **Yan Zhou:** Writing – original draft, Methodology, Formal analysis, Data curation. **Di Zhu:** Software, Formal analysis, Data curation. **Xing Fu:** Software, Formal analysis,
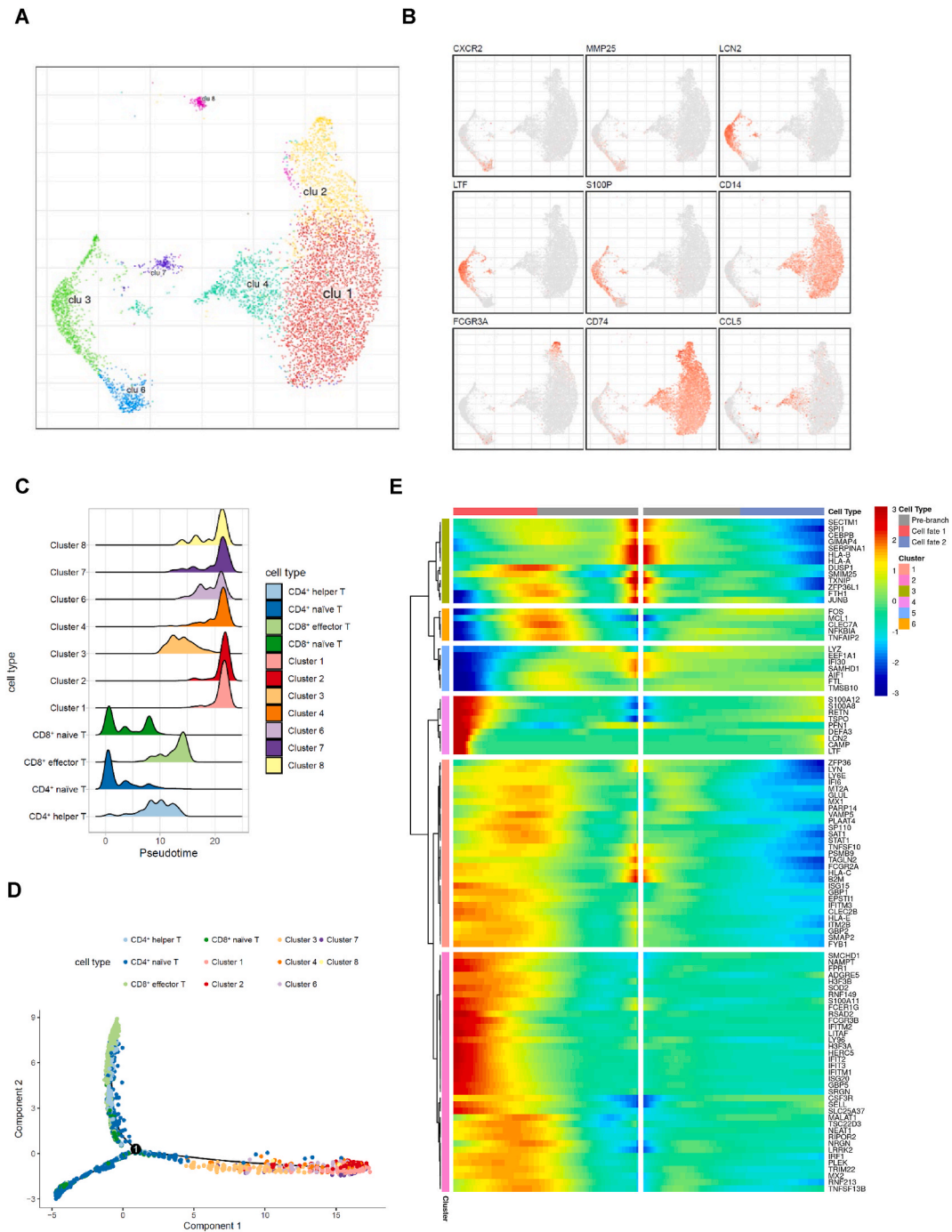
Fig. 5. Evolutionary relationship between CD8$^+$ T cells and myeloid cells in CAL patients

A. Re-cluster analysis of myeloid cells. **B.** Identification of marker genes for each myeloid cell cluster. **C.** Analysis of the evolutionary relationship between T cells and myeloid cells. **D.** Developmental trajectories of T cell clusters and myeloid cell clusters. **E.** Pseudo-temporal expression dynamics of the top 100 fate-determining genes involved in pre-branch differentiation into myeloid cluster 3 and myeloid cluster 6.
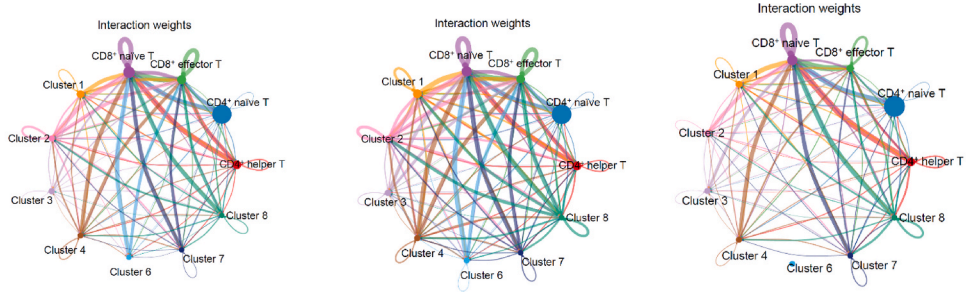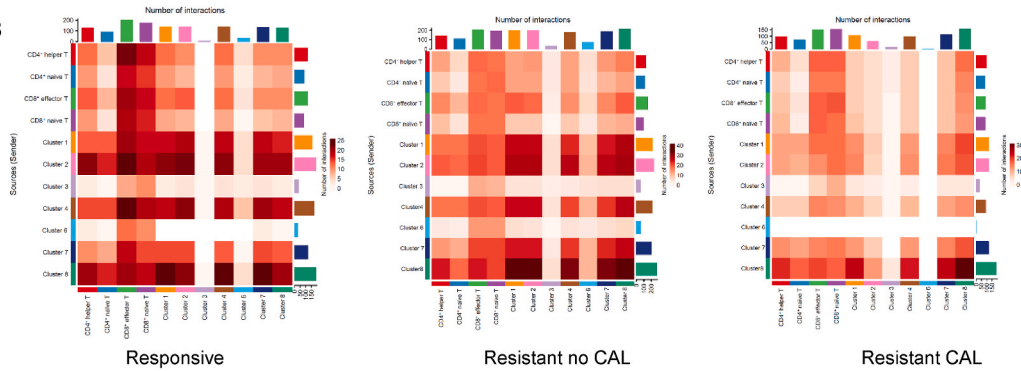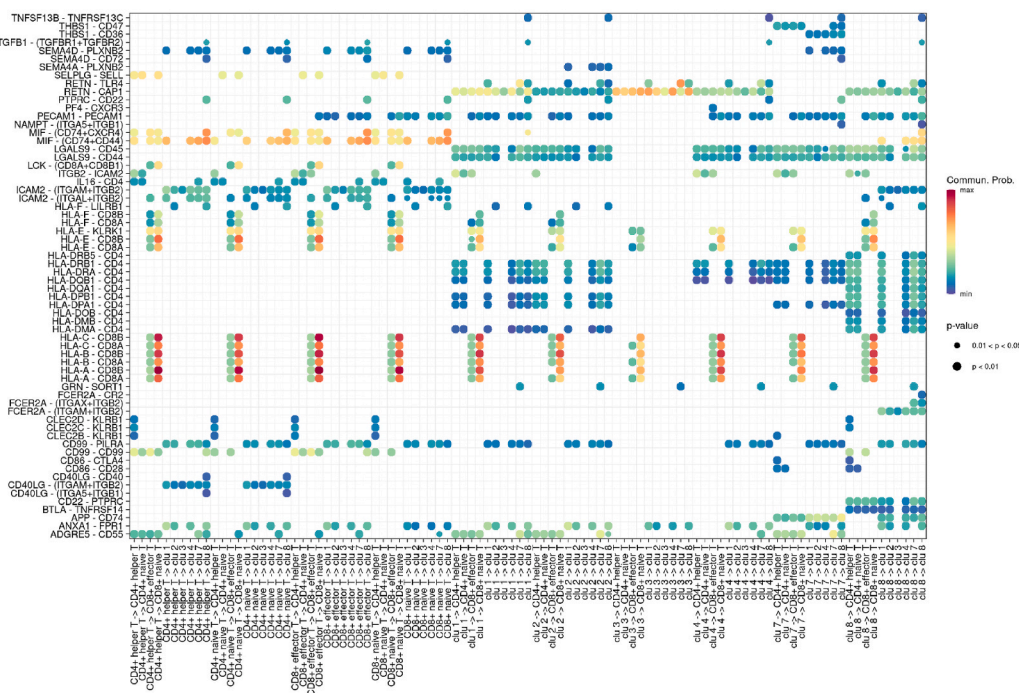
Fig. 6. Crosstalk between CD8$^+$ T cells and myeloid cells in CAL patients
A. Mutual intensity/probability map of cell-cell interaction networks between T cells and myeloid cells. Circles of different colors on the periphery indicate the number of cells, with circle size directly proportional to the cell count. Cells that emit arrows express ligands, while those that receive arrows express receptors. A higher number of ligand-receptor pairs is represented by thicker lines. **B.** Heatmap showing interaction numbers between T cells and myeloid cells. **C.** Bubble chart showing the ligand-receptor pairs interacting between T cells and myeloid cells, where a deeper red hue indicates a higher contribution value. The bubble size represents interaction probability, with *P* < 0.05 considered statistically significant.
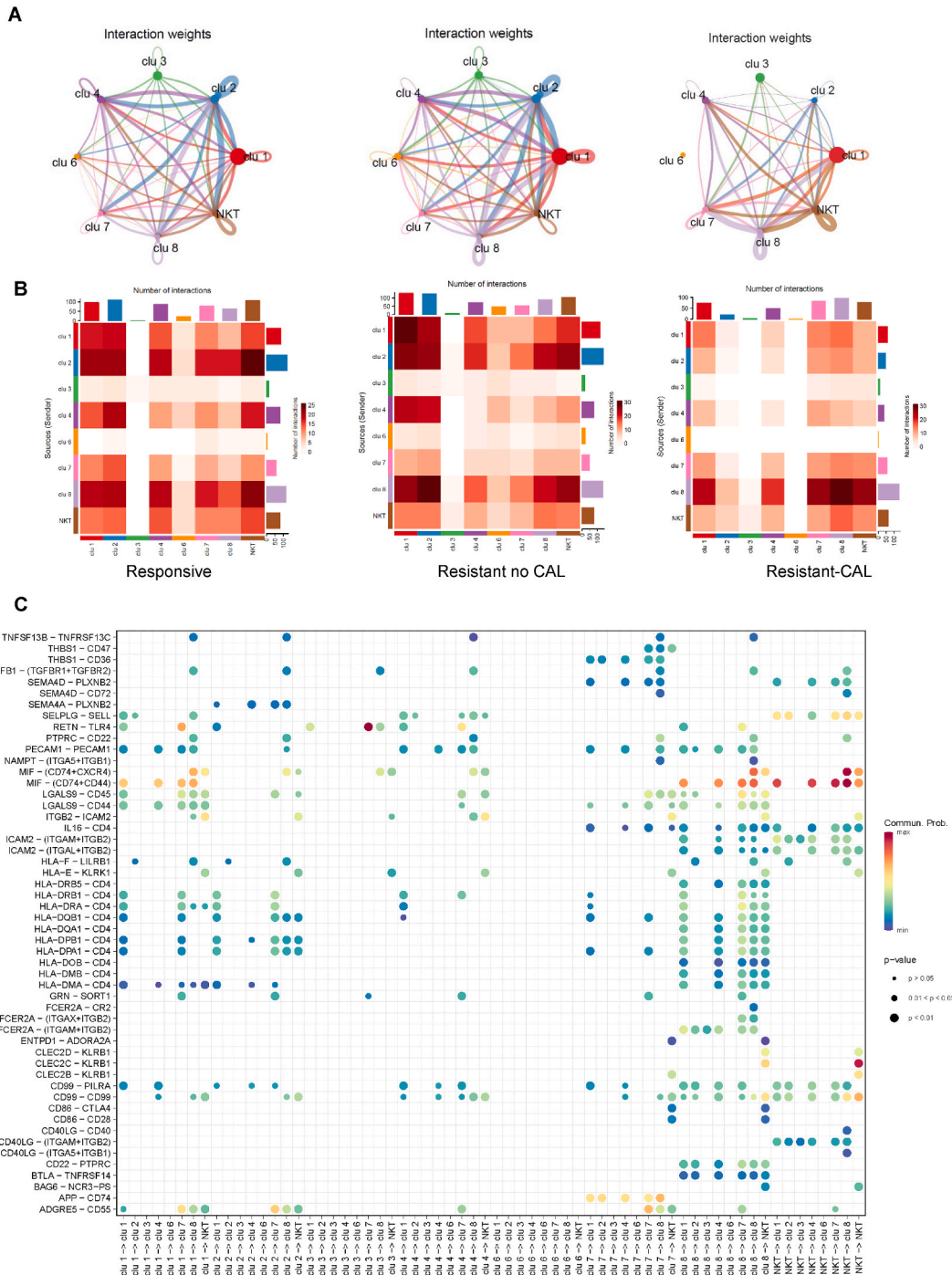
Fig. 7. Crosstalk between NKT cells and myeloid cells in CAL patients
A. Mutual intensity/probability map of cell-cell interaction networks between NKT cells and myeloid cells. Circles of different colors on the periphery indicate the number of cells, with circle size directly proportional to cell count. Cells emitting arrows express ligands, while those receiving arrows express receptors, with thicker lines representing a greater number of ligand-receptor pairs. **B.** Heatmap displaying interaction numbers between NKT cells and myeloid cells. **C.** Bubble chart illustrating the ligand-receptor interactions between NKT cells and myeloid cells, where a deeper red hue indicates a higher contribution value. The bubble size represents interaction probability, with $P < 0.05$ considered statistically significant.

Declaration of competing interest

The authors declare that they have no conflict of interest.

Acknowledgments

Appendix A. Supplementary data

Supplementary data to this article can be found online at https://doi.org/10.1016/j.heliyon.2024.e37857.

References

[1] J.C. Burns, The etiologies of Kawasaki disease, J. Clin. Invest. 134 (2024), https://doi.org/10.1172/jci176938.
[2] B.W. McCrindle, A.H. Rowley, J.W. Newburger, et al., Diagnosis, treatment, and long-term management of Kawasaki disease: a scientific statement for health professionals from the American heart association, Circulation 135 (2017) e927–e999, https://doi.org/10.1161/CIR.0000000000000484.
[3] N. Makino, Y. Nakamura, M. Yashiro, et al., Descriptive epidemiology of Kawasaki disease in Japan, 2011-2012: from the results of the 22nd nationwide survey, J. Epidemiol. 25 (2015) 239–245, https://doi.org/10.2188/jea.JE20140089.
[4] R. Ae, N. Makino, K. Kosami, et al., Epidemiology, treatments, and cardiac complications in patients with Kawasaki disease: the nationwide survey in Japan, 2017-2018, J. Pediatr. 225 (2020) 23–29 e22, https://doi.org/10.1016/j.jpeds.2020.05.034.
[5] J. Kim, K. Hong, D. Yoo, B.C. Chun, Spatiotemporal clusters of Kawasaki disease in South Korea from 2008 to 2017: a municipal-level ecological study, Frontiers in Pediatrics 10 (2023), https://doi.org/10.3389/fped.2022.1054985.
[6] K. Miyata, E.V. Bainto, X. Sun, et al., Infliximab for intensification of primary therapy for patients with Kawasaki disease and coronary artery aneurysms at diagnosis, Arch. Dis. Child. 108 (2023) 833–838, https://doi.org/10.1136/archdischild-2023-325639.
[7] R. Fukazawa, J. Kobayashi, M. Ayusawa, et al., JCS/JSCS 2020 guideline on diagnosis and management of cardiovascular sequelae in Kawasaki disease, Circ. J. 84 (2020) 1348–1407, https://doi.org/10.1253/circj.CJ-19-1094.
[8] N. Advani, S. Sastroasmoro, T. Ontoseno, C.S. Uiterwaal, Long-term outcome of coronary artery dilatation in Kawasaki disease, Ann. Pediatr. Cardiol. 11 (2018) 125–129, https://doi.org/10.4103/apc.APC_172_16.
[9] Y. Kuniyoshi, Y. Tsujimoto, M. Banno, et al., Prediction models for intravenous immunoglobulin resistance in Kawasaki disease: a meta-analysis, Pediatrics 151 (5) (2023) e2022059175, https://doi.org/10.1542/peds.2022-059175.
[10] U. Kaya Akca, E. Arslanoglu Aydin, H.H. Aykan, et al., Comparison of IVIG resistance predictive models in Kawasaki disease, Pediatr. Res. 91 (2021) 621–626, https://doi.org/10.1038/s41390-021-01459-w.
[11] S. Wang, H. Huang, M. Hou, et al., Risk-prediction models for intravenous immunoglobulin resistance in Kawasaki disease: risk-of-Bias Assessment using PROBAST, Pediatr. Res. 94 (2023) 1125–1135, https://doi.org/10.1038/s41390-023-02558-6.
[12] K.B. Dummer, K. Miyata, C. Shimizu, et al., DOACs in patients with giant coronary artery aneurysms after Kawasaki disease, JAMA Netw. Open 6 (2023), https://doi.org/10.1001/jamanetworkopen.2023.43801.
[13] M. Noval Rivas, M. Arditi, Kawasaki disease: pathophysiology and insights from mouse models, Nat. Rev. Rheumatol. 16 (2020) 391–405, https://doi.org/10.1038/s41584-020-0426-0.
[14] K. Suda, M. Iemura, H. Nishiono, et al., Long-term prognosis of patients with Kawasaki disease complicated by giant coronary aneurysms: a single-institution experience, Circulation 123 (2011) 1836–1842, https://doi.org/10.1161/CIRCULATIONAHA.110.978213.
[15] V. Shah, G. Christov, T. Mukasa, et al., Cardiovascular status after Kawasaki disease in the UK, Heart 101 (2015) 1646–1655, https://doi.org/10.1136/heartjnl-2015-307734.
[16] S. Wang, S.T. Sun, X.Y. Zhang, et al., The evolution of single-cell RNA sequencing technology and application: progress and perspectives, Int. J. Mol. Sci. 24 (2023), https://doi.org/10.3390/ijms24032943.
[17] I. Kang, R. Bucala, The immunobiology of MIF: function, genetics and prospects for precision medicine, Nat. Rev. Rheumatol. 15 (2019) 427–437, https://doi.org/10.1038/s41584-019-0238-2.
[18] J.B. Bilsborrow, E. Doherty, P.V. Tilstam, R. Bucala, Macrophage migration inhibitory factor (MIF) as a therapeutic target for rheumatoid arthritis and systemic lupus erythematosus, Expert Opin. Ther. Targets 23 (2019) 733–744, https://doi.org/10.1080/14728222.2019.1656718.
[19] E.F. Morand, M. Leech, J. Bernhagen, MIF: a new cytokine link between rheumatoid arthritis and atherosclerosis, Nat. Rev. Drug Discov. 5 (2006) 399–411, https://doi.org/10.1038/nrd2029.
[20] O. Lyudovyk, J.Y. Kim, D. Qualls, et al., Impaired humoral immunity is associated with prolonged COVID-19 despite robust CD8 T cell responses, Cancer Cell 40 (2022) 738–753.e735, https://doi.org/10.1016/j.ccell.2022.05.013.
[21] T. Kawasaki, M. Ikegawa, K. Yunoki, et al., Alveolar macrophages instruct CD8(+) T cell expansion by antigen cross-presentation in lung, Cell Rep. 41 (2022) 111828, https://doi.org/10.1016/j.celrep.2022.111828.
[22] W. Su, J. Saravia, I. Risch, et al., CXCR6 orchestrates brain CD8(+) T cell residency and limits mouse Alzheimer's disease pathology, Nat. Immunol. 24 (2023) 1735–1747, https://doi.org/10.1038/s41590-023-01604-z.
[23] H.S. Mahdi, M. Woodall-Jappe, P. Singh, M.S. Czuczman, Targeting regulatory T cells by E7777 enhances CD8 T-cell-mediated anti-tumor activity and extends survival benefit of anti-PD-1 in solid tumor models, Front. Immunol. 14 (2023) 1268979, https://doi.org/10.3389/fimmu.2023.1268979.
[24] Z. Wang, L. Xie, G. Ding, et al., Single-cell RNA sequencing of peripheral blood mononuclear cells from acute Kawasaki disease patients, Nat. Commun. 12 (2021) 5444, https://doi.org/10.1038/s41467-021-25771-5.
[25] Y. Sugitani, K. Furuno, K. Sueishi, T. Hara, Macrophages and cytotoxic T cells infiltrate the destructed mitral tissue in Kawasaki disease, BMJ Case Rep. 2018 (2018), https://doi.org/10.1136/bcr-2017-223584.
[26] M.J. Molloy, K.A. Auger, M. Hall, et al., Epidemiology and severity of illness of MIS-C and Kawasaki disease during the COVID-19 pandemic, Pediatrics 152 (5) (2023) e2023062101, https://doi.org/10.1542/peds.2023-062101.
[27] N.D. Beckmann, P.H. Comella, E. Cheng, et al., Downregulation of exhausted cytotoxic T cells in gene expression networks of multisystem inflammatory syndrome in children, Nat. Commun. 12 (2021), https://doi.org/10.1038/s41467-021-24981-1.

[28] P. Tsoukas, R.S.M. Yeung, Kawasaki disease and MIS-C share a host immune response, Nat. Rev. Rheumatol. 18 (2022) 555–556, https://doi.org/10.1038/s41584-022-00820-5.

[29] L. Schindler, L.C.D. Smyth, J. Bernhagen, M.B. Hampton, N. Dickerhof, Macrophage migration inhibitory factor (MIF) enhances hypochlorous acid production in phagocytic neutrophils, Redox Biol. 41 (2021), https://doi.org/10.1016/j.redox.2021.101946.

[30] S. Djudjaj, H. Lue, S. Rong, et al., Macrophage migration inhibitory factor mediates proliferative GN via CD74, J. Am. Soc. Nephrol. 27 (2016) 1650–1664, https://doi.org/10.1681/ASN.2015020149.

[31] X. Shi, L. Leng, T. Wang, et al., CD44 is the signaling component of the macrophage migration inhibitory factor-CD74 receptor complex, Immunity 25 (2006) 595–606, https://doi.org/10.1016/j.immuni.2006.08.020.

[32] S.C. Donnelly, Macrophage migration inhibitory factor (MIF) and severe acute COVID-19 infection, QJM 116 (2023) 159–160, https://doi.org/10.1093/qjmed/hcad033.

[33] L. Zhu, X. Xie, L. Zhang, et al., TBK-binding protein 1 regulates IL-15-induced autophagy and NKT cell survival, Nat. Commun. 9 (2018), https://doi.org/10.1038/s41467-018-05097-5.

[34] S.W. Lee, H.J. Park, L. Van Kaer, S. Hong, Roles and therapeutic potential of CD1d-Restricted NKT cells in inflammatory skin diseases, Front. Immunol. 13 (2022) 979370, https://doi.org/10.3389/fimmu.2022.979370.

[35] Y. Li, P. Kanellakis, H. Hosseini, et al., A CD1d-dependent lipid antagonist to NKT cells ameliorates atherosclerosis in ApoE-/- mice by reducing lesion necrosis and inflammation, Cardiovasc. Res. 109 (2016) 305–317, https://doi.org/10.1093/cvr/cvv259.